

RESEARCH ARTICLE

Spatio-temporal quantile regression analysis revealing more nuanced patterns of climate change: A study of long-term daily temperature in Australia

Qibin Duan , Clare A. McGrory, Glenn Brown, Kerrie Mengersen, You-Gan Wang *

School of Mathematical Sciences, Queensland University of Technology, Brisbane, Australia

* you-gan.wang@qut.edu.au OPEN ACCESS

Citation: Duan Q, McGrory CA, Brown G, Mengersen K, Wang Y-G (2022) Spatio-temporal quantile regression analysis revealing more nuanced patterns of climate change: A study of long-term daily temperature in Australia. PLoS ONE 17(8): e0271457. <https://doi.org/10.1371/journal.pone.0271457>

Editor: Shamsuddin Shahid, Universiti Teknologi Malaysia, MALAYSIA

Received: November 15, 2021

Accepted: June 30, 2022

Published: August 24, 2022

Copyright: © 2022 Duan et al. This is an open access article distributed under the terms of the [Creative Commons Attribution License](https://creativecommons.org/licenses/by/4.0/), which permits unrestricted use, distribution, and reproduction in any medium, provided the original author and source are credited.

Data Availability Statement: All data files are available to download from the R package (bomrange) on GitHub (<https://github.com/ropensci/bomrang>).

Funding: ARC Centre of Excellence for Mathematical and Statistical Frontiers (ACEMS) CE140100049 - YG & KM.

Competing interests: The authors have declared that no competing interests exist.

Abstract

Many studies have considered temperature trends at the global scale, but the literature is commonly associated with an overall increase in mean temperature in a defined past time period and hence lacking in in-depth analysis of the latent trends. For example, in addition to heterogeneity in mean and median values, daily temperature data often exhibit quasi-periodic heterogeneity in variance, which has largely been overlooked in climate research. To this end, we propose a joint model of quantile regression and variability. By accounting appropriately for the heterogeneity in these types of data, our analysis using Australian data reveals that daily maximum temperature is warming by $\sim 0.21^\circ\text{C}$ per decade and daily minimum temperature by $\sim 0.13^\circ\text{C}$ per decade. More interestingly, our modeling also shows nuanced patterns of change over space and time depending on location, season, and the percentiles of the temperature series.

Introduction

The increase in the intensity and frequency of global extreme weather events, e.g., extreme heat, extreme cold, drought, snow cover decline, is attributed to fundamental changes in the underlying climate [1, 2]. There is also an overall warming trend occurring with the global mean temperature estimated to have risen by 0.85°C during 1880–2012 [3]. This increasing trend is predicted to continue. These changes have already caused and will continue to induce substantial societal and ecological impacts. Unchecked, climate change is hence a major threat now faced by the entire world.

As the study [4] highlights, the global surface warming of recent decades has been realized as a succession of periods of warming slowdowns, or hiatus, followed by warming surges. While warming is the trend globally, at the regional and local scales, a wide variety of changes in temperature is observable across the globe [5, 6]. Climate changes have been extensively studied at the global scale, but there is also intense interest in understanding patterns of change at a national level [7].

Australia is the largest country in Oceania and one of the major producers of agricultural products, so deep understanding of climate change in Australia is important. According to the State of the Climate [8], Australia's climate has warmed on average by $1.44 \pm 0.24^\circ\text{C}$ since 1910, with most of the warming having occurred since 1950. This has been accompanied by increased frequency of extreme heat events. As reported in more detail in the Climate Statement [9], the overall mean (average of daily maximum and minimum) temperature for the 10 year period from 2010 to 2019 was the highest on record, at 0.86°C above the long term overall average since 1910, and 0.31°C warmer than the 10 years 2000–2009, which is the second warmest 10-year period. The climate change within Australia is also spatially varied. For example, for the wet tropical area in far North Queensland, the mean temperature increased by 1.1°C between 1910 and 2013 using a linear trend, while in the east coast area in New South Wales, the mean temperature increased by 0.8°C in the same period. Moreover, for the Rangelands area, the north part increased 1°C and the south part increased 0.9°C during the same period [10].

The majority of statistical analyses undertaken in climate studies in Australia are based on inference about the maximum, minimum or mean temperature. However, a focus on these measure alone can fail to detect more nuanced patterns of change over space and time. In this article we proposed an approach based on quantile regression estimates of the data with consideration of spatial correlation. Quantile regression was originally proposed by Koenker and Bassett (1978) as an alternative approach to mean regression that does not require the usual strict assumption about normally distributed residuals in the regression models [11]. The idea has been used to identify changes over time of any percentiles of climate variables; see [12–15] for particular focus on the analysis of temperature series. The performance of quantile regression for trend detection analysis has been favorably compared with traditional approaches, such as robust linear regression and the nonparametric M-K test [14]. The spatial and temporal variation can be modeled jointly as in Reich (2012), in a Bayesian manner [16].

One advantage of this approach is that quantile regression estimates are less influenced by extreme outliers in the response measurements than standard linear regression estimates based on the mean. Another substantial motivation for this approach is that the conditional quantile functions provide a variety of measures of central tendency and statistical dispersion that allow us to describe the relationship at different points in the conditional distribution of the outcome. In this way we obtain a more comprehensive picture of the relationship between the variables. When using quantile regression, we have increased freedom in our modelling in that we are not restricted by the assumption that variable relationships are the same at the median and tails of the distribution as they are at the mean. Such models could provide a more in-depth understanding of the historic change in Australian temperature, which can potentially improve anticipation and management of climate risk and associated negative impacts.

We highlight however, that in analysis of daily Australia temperature data, complicated heterogeneity in variance arises and this must be addressed if results are to be reliable. In this article we address that by proposing a joint model including variance as a covariate in our spatio-temporal regression.

Data and methods

Data collection and selection

The geographical boundary of Australia is between $9^\circ - 44^\circ\text{S}$ latitude and $112^\circ - 154^\circ\text{E}$ longitude (apart from Macquarie Island), with total area of $7,692,024\text{ km}^2$. The massive size of the country gives it a wide variety of landscapes, with tropical rainforests in the north-east, mountain ranges in the south-east, south-west and east, and desert and semi-arid land in the center,

resulting in a variety of climates across the country. The northern part of the country has a tropical climate, with predominantly summer rainfall. As for the southern part, the south-west corner of the country has a Mediterranean climate, while the south-east ranges from oceanic (Tasmania and coastal Victoria) to humid subtropical (from the upper half of New South Wales), with highlands featuring alpine and subpolar oceanic climates. The interior desert has stable arid and semi-arid climates. More details about the Australian climate can be found on the website of Bureau of Meteorology (BoM), Australia [17].

The daily maximum (Dmx) and minimum (Dmn) temperature series were obtained from 1,745 weather stations operated by the BoM Australia. These datasets can be accessed through the R package `bomrang` [18]. The length of these time series varies among different stations from less than 10 years to more than 100 years of observations. The latitude, longitude and elevations of each station are also obtained from the BoM website.

We restricted the study period from Jan 1, 1960 to Dec 31, 2019, so that most warming periods can be covered and more operating stations could be included [19]. As the years of 2000 and 2010 are the starting years of the top two warmest 10-year periods in Australia on record, we considered data from stations not covering these periods to be less meaningful in terms of studying the warming trend in Australia. Therefore, we excluded stations that were not operating during these periods. Furthermore, we excluded the stations with over 20% missing observations or with 5 years continuous missing observations. As a result, data from 72 stations were included in our analysis and missing observations of these stations were interpolated using ordinary kriging [20]. These stations are geographically distributed as shown in Fig 1. Specifically, there are 22 stations in Queensland (QLD), 18 in Western Australia (WA), 11 in New south Wales (NSW), 9 in Victoria (VIC), 7 South Australia (SA), 4 in Tasmania (TAS) and 2 in the Northern Territory (NT). The ID number of each station is also included for the sake of description of results.

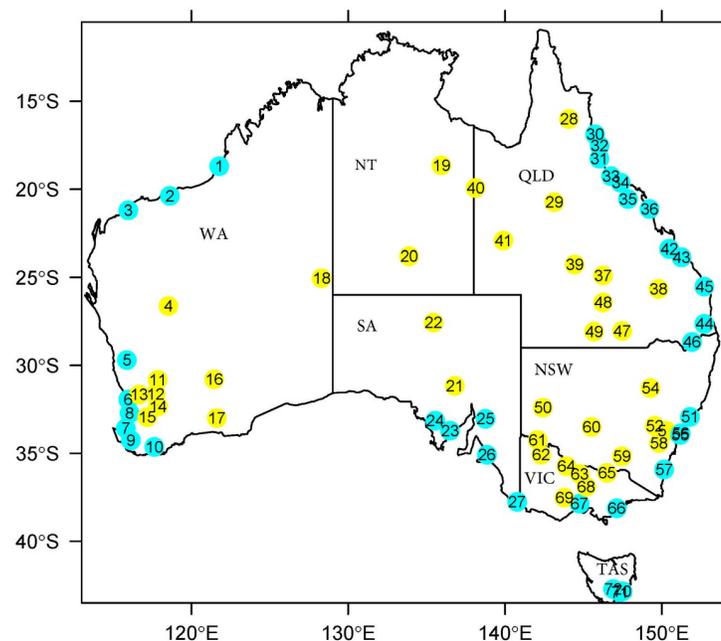


Fig 1. The distribution of selected stations with qualifying data. Blue dots are for (near) coastal stations and yellow dots are for inland stations.

<https://doi.org/10.1371/journal.pone.0271457.g001>

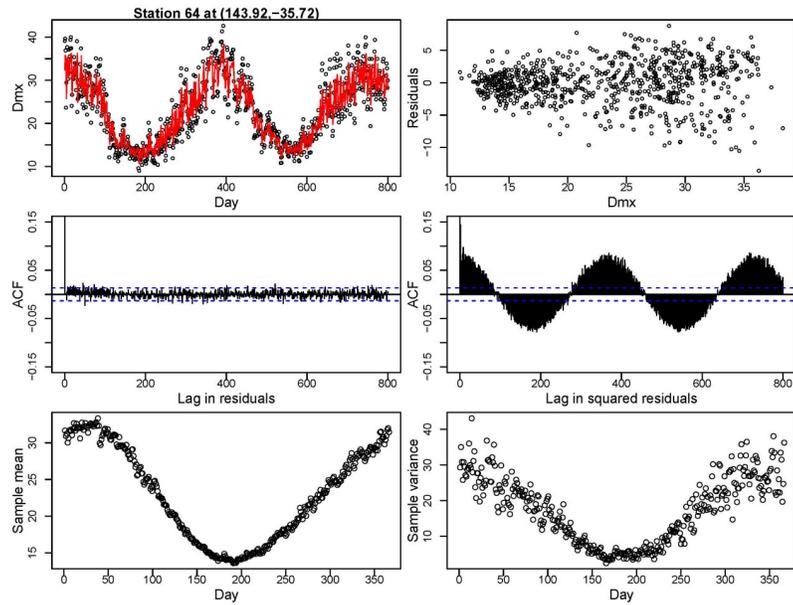


Fig 2. Exploratory analysis for a single station. Top left: fitting parametric mean model for Dmx. Top right: residuals of fit against predicted Dmx for the parametric mean model. Middle left: Auto-Correlation Function (ACF) plot for residuals for lag up to 800 days. Middle right: ACF plot for squared residuals for lag up to 800 days. Bottom left: sample mean over 60 years. Bottom right: sample variance over 60 years.

<https://doi.org/10.1371/journal.pone.0271457.g002>

Exploratory analysis

The daily temperature time series are affected by seasonality, with quasi-periodic variations in both sample mean and variance; see [21–24]. An example is shown in the bottom panels in Fig 2, where the sample mean and variance of a particular station are calculated over 60 years of observations. Other stations had different patterns, depending on the respective ecosystem, but they similarly exhibited this phenomenon.

Such mean periodicity in the series can be handled with parametric harmonic functions (or truncated Fourier series). Ignoring the seasonality or heterogeneity in variance for the time being, the observed daily temperature time series can be modelled as follows.

$$y_t(\mathbf{s}) = \mu_t(\mathbf{s}) + \sigma(\mathbf{s})\epsilon_t(\mathbf{s}), \quad \epsilon_t(\mathbf{s}) \sim_{iid} N(0, 1), \tag{1}$$

where t is t -th day from January 1, 1960 to December 31, 2019, \mathbf{s} is a particular station, and expected value $\mu_t(\mathbf{s})$ is given by

$$\mu_t(\mathbf{s}) = \beta_0(\mathbf{s}) + \beta_1(\mathbf{s})t + \beta_2(\mathbf{s})\mathbf{x}_t(\mathbf{s}) + FSk(t, \mathbf{a}(\mathbf{s}), \mathbf{b}(\mathbf{s})) + \sum_{i=1}^p \rho_i(\mathbf{s})e_{t-i}(\mathbf{s}). \tag{2}$$

Note that $\epsilon_t(\mathbf{s})$ is assumed to be white noise and small-scaled relative to the scale of $\mu_t(\mathbf{s})$ and $\sigma^2(\mathbf{s})$ is constant in location \mathbf{s} . Here $FSk(t, \mathbf{a}(\mathbf{s}), \mathbf{b}(\mathbf{s}))$ is the k -th order truncated Fourier series, and $\sum_{i=1}^p \rho_i(\mathbf{s})e_{t-i}(\mathbf{s})$ is an $AR(p)$ process. The term $\beta_2(\mathbf{s})\mathbf{x}_t(\mathbf{s})$ is the term for other covariates, and in the following we consider the inclusion of the Southern Oscillation Index (SOI) values. For simplicity of notation, we denote the k th order truncated Fourier series as follows

$$FSk(t, \mathbf{a}(\mathbf{s}), \mathbf{b}(\mathbf{s})) = \sum_{j=1}^k \left[a_j(\mathbf{s}) \sin\left(\frac{2\pi jt}{D_t}\right) + b_j(\mathbf{s}) \cos\left(\frac{2\pi jt}{D_t}\right) \right],$$

where $\mathbf{a}(\mathbf{s}) = (a_1(\mathbf{s}), \dots, a_k(\mathbf{s}))$ and $\mathbf{b}(\mathbf{s}) = (b_1(\mathbf{s}), \dots, b_k(\mathbf{s}))$ are the coefficients of harmonic terms for station \mathbf{s} , and D_t denotes the number of days in the respective year.

The red curve in the top left panel of Fig 2 shows the fitted values of $\mu_t(\mathbf{s})$ for one station for illustration; these are obtained from the model in Eq (1). The top right panel shows the residuals against fitted values which clearly indicate the heterogeneity issue in the variance. This leads to the failure of the equal variance assumption in Eq (1). Tests of temporal auto-correlation are shown in the middle panels: for this station, no substantial auto-correlation is found for the residuals, while significant and quasi-periodic auto-correlation is found in the squared residuals.

Although the heterogeneity issue is not emphasized and indeed often ignored in many climate themed articles, some models have been proposed to address it. For instance, in the model of the daily average temperature of four US cities, heterogeneity of variance is accounted for via a GARCH process [21]. In some studies, for example, ARCH models were employed [22, 23, 25], while Sirangelo (2017) models the inter-annual sample variance $\hat{\sigma}_d^2(\mathbf{s})$ as simple periodic functions [24].

In this study, we model the variance of daily temperature with the inter-annual sample variance. Let $y_{i,d}(\mathbf{s})$ be the maximum (or minimum) daily temperature on the d -th day of year i recorded at station \mathbf{s} . Note that we assume there are 365 days for each year and February the 29th was omitted in the analysis.

For each particular day, d , for station \mathbf{s} , we compute the inter-annual sample mean and variance, denoted as $\hat{\mu}_d(\mathbf{s})$ and $\hat{\sigma}_d^2(\mathbf{s})$ respectively:

$$\hat{\mu}_d(\mathbf{s}) = \frac{1}{T} \sum_{i=1}^T y_{i,d}(\mathbf{s}), \quad \hat{\sigma}_d^2(\mathbf{s}) = \frac{\sum_{i=1}^T (y_{i,d}(\mathbf{s}) - \hat{\mu}_d(\mathbf{s}))^2}{T - 1}, \tag{3}$$

where T is number of years that are included in the analysis.

The inter-annual mean is modeled as follows

$$\mu_d(\mathbf{s}) = \hat{\mu}_d(\mathbf{s}) + \epsilon_d(\mathbf{s}), \tag{4}$$

where $\epsilon_d(\mathbf{s}) = \hat{\sigma}_d(\mathbf{s})\delta_d(\mathbf{s})$ and $\delta_d(\mathbf{s}) \sim_{iid} N(0, 1)$. We include the inter-annual mean and squared mean as a covariate of the variance function at the end of the equation below. The model selection results can be found in the S1 Supplementary Document Section in S1 File.

$$\log(\sigma_d^2(\mathbf{s})) = \beta_0(\mathbf{s}) + \beta_1(\mathbf{s})\mu_d(\mathbf{s}) + \beta_2(\mathbf{s})\mu_d^2(\mathbf{s}) + FSk(d, \mathbf{a}(\mathbf{s}), \mathbf{b}(\mathbf{s})) + \rho_1(\mathbf{s})(\hat{\sigma}_{d-1}^2(\mathbf{s}) - \sigma_{d-1}^2(\mathbf{s})). \tag{5}$$

We have tested and compared a number of variance models to account for the inter-annual heterogeneity that varies from site to site. Different orders of Fourier series have been tested and selected as $k = 4$. Quantile regression requires the heterogeneity function at each quantile level (except $\tau = 0.50$), so we need to jointly estimate the regression parameters and variance parameters.

Joint models for quantile regression and variability

Quantile regression permits simultaneous analysis of several features of the response distribution. To jointly model all quantiles simultaneously and spatially, while accounting for heterogeneity, we propose here an improved version of the spatio-temporal quantile regression approach proposed by Reich (2012) and apply it to the Australian daily temperature data [16].

Considering heterogeneity in variance, the model in Eq (1) can be modified as follows:

$$y_t(\mathbf{s}) = \mu_t(\mathbf{s}) + \sigma_t(\mathbf{s})\epsilon_t(\mathbf{s}), \quad \epsilon_t(\mathbf{s}) \sim_{iid} f(\mathbf{s}), \tag{6}$$

where $f(\mathbf{s})$ is the PDF of $\epsilon_t(\mathbf{s})$; we denote $F(\mathbf{s}) \in [0, 1]$ to be the corresponding CDF at location \mathbf{s} .

The quantile function $q(\tau|\mathbf{s}, t)$ is the function that satisfies $\mathbb{P}\{y_t(\mathbf{s}) < q(\tau|\mathbf{s}, t)\} = \tau \in [0, 1]$. Inserting Eq (6) into this expression we have $\mathbb{P}\{\mu_t(\mathbf{s}) + \sigma_t(\mathbf{s})\epsilon_t(\mathbf{s}) < q(\tau|\mathbf{s}, t)\} = \tau$ and the quantile function $q(\tau|\mathbf{s}, t)$ can be expressed as follows:

$$q(\tau|\mathbf{s}, t) = \mu_t(\mathbf{s}) + \sigma_t(\mathbf{s})F^{-1}(\tau), \tag{7}$$

where $F^{-1}(\tau)$ is the inverse CDF. If the error term $\epsilon_t(\mathbf{s})$ is assumed normally distributed, then $F^{-1}(\tau) = \Phi^{-1}(\tau)$. In this study, we are interested in testing the changes in the quantile function $q(\tau|\mathbf{s}, t)$ over time t for each τ . Therefore, in Eq (7), the term $\sigma_t(\mathbf{s})$ needs to account for the time variable t . For example, for the case of a Gaussian distributed response with linear trend over time in Chandler (2005), the mean is modeled as $\mu_t(\mathbf{s}) = \beta_0(\mathbf{s}) + \beta_1(\mathbf{s})t$, and the standard deviation $\sigma_t(\mathbf{s}) = \theta_0(\mathbf{s}) + \theta_1(\mathbf{s})t$, with $F^{-1}(\tau) = \Phi^{-1}(\tau)$ [26]. Here, the standard deviation changes linearly with time t . The Gaussian assumption is generalized by Reich (2012), by incorporating a piece-wise Gaussian basis function to describe the linearly changing heterogeneity more flexibly for a non-Gaussian distributed response [16]. Furthermore, this model is able to characterize the entire quantile process with accommodation of non-Gaussian features, such as asymmetry and heavy or light tails. However, the model of Reich (2012) was proposed for a set of annual monthly temperature data without consideration of seasonality in mean and variance. Therefore, it is not applicable to daily temperature data.

Next, we will describe our generalized model which is suitable for daily temperature data. Note that the model is specifically tailored for trend detection so that the time period t is confined within $[0, 1]$ to satisfy the constraints of a quantile function $q(\tau|\mathbf{s}, t)$ increasing in τ as suggested in Reich (2012). A model that is directly derived from Reich (2012) is as follows in Eq (8).

Let $0 = \kappa_1 < \dots < \kappa_{L+1} = 1$ be a grid of equally spaced knots covering $[0, 1]$. Then, for l with $\kappa_l < 0.5$,

$$B_l(\tau) = \begin{cases} \Phi^{-1}(\kappa_l) - \Phi^{-1}(\kappa_{l+1}) & \text{if } \tau < \kappa_l \\ \Phi^{-1}(\tau) - \Phi^{-1}(\kappa_{l+1}) & \text{if } \kappa_l \leq \tau < \kappa_{l+1} \\ 0 & \text{if } \kappa_{l+1} \leq \tau \end{cases}$$

and, for l such that $\kappa_l \geq 0.5$,

$$B_l(\tau) = \begin{cases} 0 & \text{if } \tau < \kappa_l \\ \Phi^{-1}(\tau) - \Phi^{-1}(\kappa_{l+1}) & \text{if } \kappa_l \leq \tau < \kappa_{l+1} \\ \Phi^{-1}(\kappa_{l+1}) - \Phi^{-1}(\kappa_l) & \text{if } \kappa_{l+1} \leq \tau \end{cases}$$

Each quantile is assumed to be a function of time t for each station as follows:

$$q(\tau|\mathbf{s}, t) = g_0(\tau|\mathbf{s}) + g_1(\tau|\mathbf{s})t + g_2(\tau|\mathbf{s})x_{soi} + FSk(t, \mathbf{g}_s(\tau|\mathbf{s}), \mathbf{g}_c(\tau|\mathbf{s})), \tag{8}$$

where $\mathbf{g}_s(\tau|\mathbf{s}) = (g_3(\tau|\mathbf{s}), \dots, g_{k+2}(\tau|\mathbf{s}))$, $\mathbf{g}_c(\tau|\mathbf{s}) = (g_{k+3}(\tau|\mathbf{s}), \dots, g_{2k+2}(\tau|\mathbf{s}))$, and for each k , $g_k(\tau|\mathbf{s})$ is taken to be linear combinations of L basis functions,

$$g_k(\tau|\mathbf{s}) = \beta_k(\mathbf{s}) + \sum_{l=1}^L B_l(\tau)\theta_{k,l}(\mathbf{s}). \tag{9}$$

The trend function $g_1(\tau|\mathbf{s})$ is of particular interest for trend detection in this study. Note that when $g_k(\tau|\mathbf{s}) = 0$ for all $k > 1$, the model in Eq (8) degenerates to a linear model that is exactly the same as that used in [16]. If further, we let $L = 1$ and $B_1(\mathbf{s}) = \Phi^{-1}(\tau)$, we obtain the special Gaussian case that corresponds to the model in [26].

Eq (8) can be further written as,

$$q(\tau|\mathbf{s}, t) = \underbrace{\beta_0(\mathbf{s}) + \beta_1(\mathbf{s})t + \beta_2(\mathbf{s})x_{soi}}_{\mu_t(\mathbf{s})} + FSk(t, \boldsymbol{\beta}_s(\mathbf{s}), \boldsymbol{\beta}_c(\mathbf{s})) + \sum_{l=1}^L B_l(\tau) \underbrace{[\theta_{0,l}(\mathbf{s}) + \theta_{1,l}(\mathbf{s})t + \theta_{2,l}(\mathbf{s})x_{soi} + FSk(t, \boldsymbol{\theta}_{s,l}(\mathbf{s}), \boldsymbol{\theta}_{c,l}(\mathbf{s}))]}_{\sigma_l(\mathbf{s}, t)}, \tag{10}$$

where $\boldsymbol{\beta}_s(\mathbf{s}) = (\beta_1(\mathbf{s}), \dots, \beta_{k+2}(\mathbf{s}))$, $\boldsymbol{\beta}_c(\mathbf{s}) = (\beta_{k+3}(\mathbf{s}), \dots, \beta_{2k+2}(\mathbf{s}))$, $\boldsymbol{\theta}_{s,l}(\mathbf{s}) = (\theta_{3,b} \dots, \theta_{k+2, l})$, and $\boldsymbol{\theta}_{c,l}(\mathbf{s}) = (\theta_{k+3, b} \dots, \theta_{2k+2, l})$. In Eq (10), $\beta_k(\mathbf{s})$, the center of the quantile function at location \mathbf{s} , and $\theta_{k,l}(\mathbf{s})$ are unknown coefficients that determine the shape of the quantile function. Here, $\boldsymbol{\beta}_s(\mathbf{s})$ is the same parameter vector with the mean regression model, e.g., $\beta_0(\mathbf{s})$ is the intercept and $\beta_1(\mathbf{s})$ is the trend coefficient.

Here, adding $FSk(t, \boldsymbol{\theta}_{s,l}(\mathbf{s}), \boldsymbol{\theta}_{c,l}(\mathbf{s}))$ terms in Eq (10) enables the model to account for seasonal heterogeneity in the variance. However, auto-correlations in both mean and variance are not considered. Moreover, the variance function also depends on the mean values according to exploratory analysis. To account for all information, we further improve the model by replacing the $\theta_{0,l}(\mathbf{s}) + FSk(t, \boldsymbol{\theta}_{s,l}(\mathbf{s}), \boldsymbol{\theta}_{c,l}(\mathbf{s}))$ with $\theta_{2k+3, l}(\mathbf{s})\sigma_{d(t)}(\mathbf{s})$ in $\sigma_l(\mathbf{s}, t)$, where $d(t)$ is the $d(t)$ -th day of a year for the t -th time point and $\sigma_{d(t)}(\mathbf{s})$ is modeled in Eq (5). The new model is given as follows

$$q(\tau|\mathbf{s}, t) = \underbrace{\beta_0(\mathbf{s}) + \beta_1(\mathbf{s})t + \beta_2(\mathbf{s})x_{soi}}_{\mu_t(\mathbf{s})} + FSk(t, \boldsymbol{\beta}_s(\mathbf{s}), \boldsymbol{\beta}_c(\mathbf{s})) + \sum_{l=1}^L B_l(\tau) \underbrace{[\theta_{1,l}(\mathbf{s})t + \theta_{2,l}(\mathbf{s})x_{soi} + \theta_{2k+3,l}(\mathbf{s})\sigma_{d(t)}(\mathbf{s})]}_{\sigma_l(\mathbf{s}, t)}. \tag{11}$$

Note that the model in Eq (11) is equivalent to adding a new term $g_{2k+3l}(\tau|\mathbf{s})\sigma_{d(t)}$ to Eq (10) and replacing the unknown parameters $(\beta_{2k+3, l}(\mathbf{s}), \theta_{0,l}(\mathbf{s}), \boldsymbol{\theta}_{s,l}(\mathbf{s}), \boldsymbol{\theta}_{c,l}(\mathbf{s}))$ by zeros. Compared with the model in Eq (10), the model in Eq (11) has far fewer unknown parameters to estimate. In both spatio-temporal quantile models Eqs (10) and (11), the quantile function can vary spatially by allowing both the $\beta_k(\mathbf{s})$ and $\theta_{k,l}(\mathbf{s})$ to be Gaussian spatial processes with exponential covariance. The β_k are independent Gaussian processes with mean $\bar{\beta}_k$ and covariance $COV(\beta_k(\mathbf{s}), \beta_k(\mathbf{s}')) = \psi_{\beta_k}^2 \exp(-\|\mathbf{s} - \mathbf{s}'\|/\rho_{\beta_k})$. The $\theta_{k,l}$ are modeled similarly with mean $\bar{\theta}_{k,l}$ and covariance $COV(\theta_{k,l}(\mathbf{s}), \theta_{k,l}(\mathbf{s}')) = \psi_{\theta_k}^2 \exp(-\|\mathbf{s} - \mathbf{s}'\|/\rho_{\theta_k})$, but they must satisfy $\sigma_l(\mathbf{s}, t) > 0$ for all l and t .

The density function of $y_l(\mathbf{s})$ can be expressed in a closed form. Firstly, the quantile function can be written as

$$q(\tau|\mathbf{s}, t) = \sum_{l=1}^L [a_l(\mathbf{s}, t) + \sigma_l(\mathbf{s}, t)\Phi^{-1}(\tau)]I_{\{\kappa_l \leq \tau < \kappa_{l+1}\}}, \tag{12}$$

where $\sigma_l(\mathbf{s}, t)$ is the coefficient of $B_l(\tau)$ and $a_l(\mathbf{s}, t) = q(\kappa_{l+1}|\mathbf{s}, t) - \sigma_l(\mathbf{s}, t)\Phi^{-1}(\kappa_{l+1})$ if $\kappa_l < 0.5$ and $a_l(\mathbf{s}, t) = q(\kappa_l|\mathbf{s}, t) - \sigma_l(\mathbf{s}, t)\Phi^{-1}(\kappa_l)$ if $\kappa_l \geq 0.5$. Then the density function of $y_l(\mathbf{s})$ is given

as follows

$$f(y_t(\mathbf{s})) = \sum_{l=1}^L I_{\{q(\kappa_l|\mathbf{s},t) < y_t(\mathbf{s}) \leq q(\kappa_{l+1}|\mathbf{s},t)\}} N(y_t(\mathbf{s})|a_l(\mathbf{s}, t), \sigma_l(\mathbf{s}, t)^2), \tag{13}$$

where $\sigma_l(\mathbf{s}, t) > 0$ for all l and t at each location \mathbf{s} .

Additional residual correlation is assumed to be an AR(1) process and handled with a copula approach using a latent residual process that is implemented in [16]. Let $v_t(\mathbf{s})$ be a latent Gaussian process modeled as follows,

$$\begin{aligned} v_1(\mathbf{s}) &= w_1(\mathbf{s}) \\ v_t(\mathbf{s}) &= \rho_v v_{t-1}(\mathbf{s}) + \sqrt{(1 - \rho_v^2)} w_t(\mathbf{s}), \quad \text{for } t > 1, \end{aligned} \tag{14}$$

where $|\rho_v| < 1$ and $w_t(\mathbf{s})$ are independent spatial process with mean 0 and covariance $COV(w_t(\mathbf{s}), w_t(\mathbf{s}')) = \exp(-\|\mathbf{s} - \mathbf{s}'\|/\psi_w)$. Here, $v_t(\mathbf{s}) \sim N(0, 1)$ for each \mathbf{s} and t , and let $u_t(\mathbf{s}) = \Phi(v_t(\mathbf{s})) \sim U(0, 1)$. Moreover, let $\tau = u_t(\mathbf{s})$ in Eq (12). Then we have

$$y_t(\mathbf{s}) = q(u_t(\mathbf{s})|\mathbf{s}, t) = \sum_{l=1}^L [a_l(\mathbf{s}, t) + \sigma_l(\mathbf{s}, t)u_t(\mathbf{s})] I_{\{\kappa_l \leq u_t(\mathbf{s}) < \kappa_{l+1}\}}, \tag{15}$$

and

$$f(y_t(\mathbf{s})) = \sum_{l=1}^L I_{\{\kappa_l \leq u_t(\mathbf{s}) < \kappa_{l+1}\}} N(y_t(\mathbf{s})|a_l(\mathbf{s}, t), \sigma_l(\mathbf{s}, t)^2). \tag{16}$$

For model inference, parameters are estimated in a Bayesian manner via the Markov chain Monte Carlo method that was implemented in Reich (2012) [16]. Note that $\beta_k(\mathbf{s})$ and $\theta_{k,l}(\mathbf{s})$ are model parameters and randomly sampled from their prior distributions (which are Gaussian spatial process) using a Gibbs sampling approach. Here random samples of $\theta_{k,l}(\mathbf{s})$ must satisfy the condition $\frac{dq(\tau|\mathbf{s},t)}{d\tau} > 0$. Hyper-parameters $\bar{\beta}_k(\mathbf{s})$ and $\bar{\theta}_{k,l}(\mathbf{s})$ are used to characterize the mean of prior distributions of $\beta_k(\mathbf{s})$ and $\theta_{k,l}(\mathbf{s})$, and $\psi_{\beta_k}, \rho_{\beta_k}, \psi_{\theta_k}$ and ρ_{θ_k} are used to characterize the respective variance. Uninformative priors for the hyper-parameters are used, where $\bar{\beta}_k$ and $\bar{\theta}_{k,l}$ have $N(0, 10^2)$ priors, and $\psi_{\beta_k}, \rho_{\beta_k}, \psi_{\theta_k}$ and ρ_{θ_k} have *InvGamma* (0.1, 0.1) priors. In the residual correlation modeling, the auto-correlation ρ_v has a $U(-1, 1)$ prior and ψ_w also has an *InvGamma*(0.1, 0.1) prior. Gibbs sampling is used for $\bar{\beta}_k(\mathbf{s}), \bar{\theta}_{k,l}(\mathbf{s})$ and ρ_v , while other spatial range hyper-parameters are updated by using Metropolis sampling with a Gaussian candidate distribution (tuned to give roughly 40% acceptance rate). Note that the estimation of $\bar{\beta}_k(\mathbf{s})$ and $\bar{\theta}_{k,l}(\mathbf{s})$ of station \mathbf{s} is also affected by the data from nearby stations, so that the heterogeneity in measurement procedure of a single station is less important. The reliability of the model is validated with a simulation study, which shows that resulting estimates of trend coefficient are very closed to the true values. A detailed description of the simulation study can be found in the S1 Supplementary Document Section in [S1 File](#).

Results

In this study we analyze the spatio-temporal pattern of warming in Australia based on the trends of averages and quantiles of daily maximum and minimum temperatures using recent observed data.

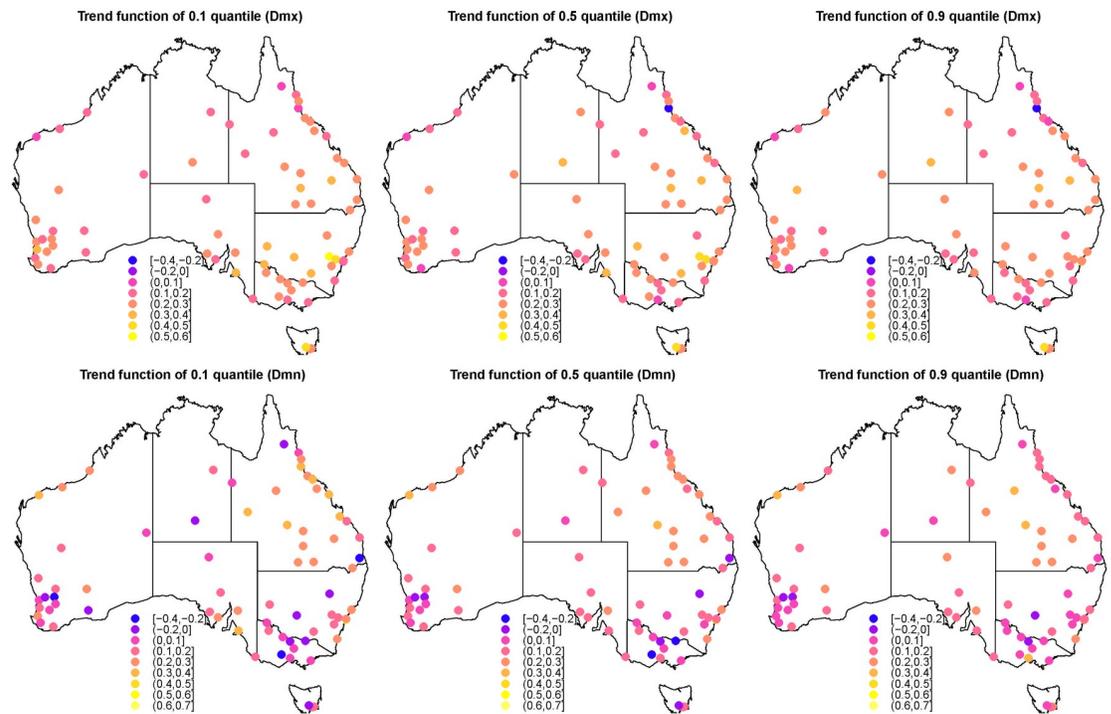


Fig 3. Quantile trend of $\tau = 0.1, 0.5$ and 0.9 for all 72 stations during the study period. The color of point is the total degrees Celsius that increased/decreased per decade from 1960 to 2019. The top panels are for the Dmx series and the bottom panels are for the Dmn series.

<https://doi.org/10.1371/journal.pone.0271457.g003>

Trend analysis based on quantiles

Fig 3 shows the values of the trend functions for quantiles 0.1, 0.5 and 0.9 for each of the included stations, respectively, while Fig 4 show the change in trend function with quantile levels for stations with any trend function $>0.3^{\circ}\text{C}$. Note that the value represents the total increases in degrees Celsius per decade during the study period of 60 years. For daily maximum temperature, the average warming trend of all 72 stations is 0.22, 0.22 and 0.20°C per decade for quantile levels 0.1, 0.5 and 0.9, respectively, while these values become 0.14, 0.13, 0.14°C for daily minimum temperature.

For all three quantile levels, the daily maximum temperatures are increasing in all stations except for one in north Queensland (station 31 in Fig 1 located in Cardwell Marine Pde QLD), and the values of the trend function per decade mostly lie in the range (0.1, 0.3) indicating a warming trend of 0.6°C to 1.8°C in total during the last 60 years. For quantile 0.1, representing cold daily maximum temperature, there are five stations in NSW that increase by more than 0.3°C per decade during the study period. Three of these (stations 50, 59 60) are within the range (0.3, 0.4) and decrease slightly to (0.2, 0.3) for larger quantiles, and another two (station 52, 53) exceed 0.4 and also decrease for higher quantiles but remain >0.2 (Fig 4). Moreover, other stations (station 38 and 48 in QLD, 8 in WA, 26 in SA, 72 in TAS) have been warming $\geq 0.3^{\circ}\text{C}$ for all three quantile levels per decade, especially for station 8 in TAS around 0.4°C . Station 61 in VIC has been warming $>0.3^{\circ}\text{C}$ for the 0.1 quantile, but this decreases to $<0.3^{\circ}\text{C}$ for higher quantiles. For quantile 0.5, representing median daily maximum temperature, there are eight stations with $>0.3^{\circ}\text{C}$ increase per decade. Of these, stations 20 in NT and 35 in QLD have smaller increases in the 0.1 quantile $<0.3^{\circ}\text{C}$ (Fig 4), and three have $>0.4^{\circ}\text{C}$ increase with two in NSW (station 52 and 53) and one (station 72) in TAS. In terms of quantile 0.9, for hot

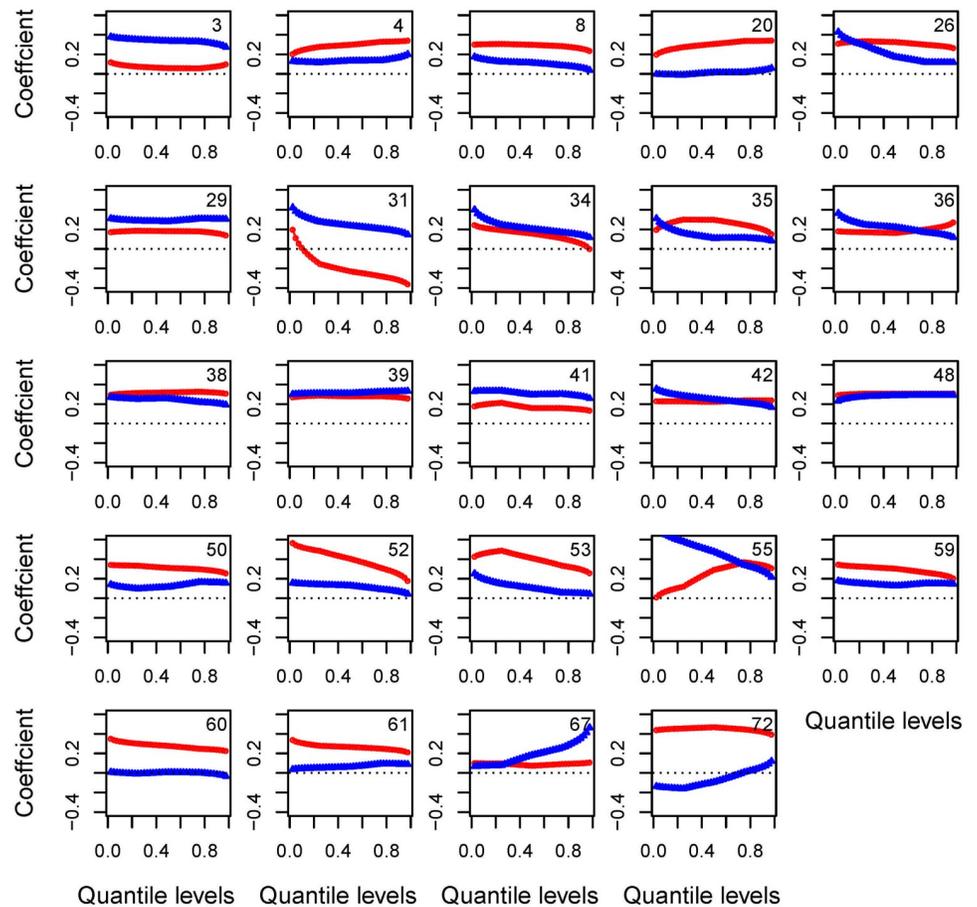


Fig 4. Quantile trend as a function of quantile level for selected stations. The red curve is for Dmx and the blue curve for Dmn. The horizontal dashed line represents coefficient being zero.

<https://doi.org/10.1371/journal.pone.0271457.g004>

daily maximum temperature, six stations show $>0.3^{\circ}\text{C}$ increase with two in QLD (station 38 and 48), and one in NSW (station 55), TAS (station 72), WA (station 4) and NT (station 20). The station 31 in QLD (located in Cardwell Marine Pde) shows a declining trend for both 0.5 and 0.9 quantiles (the top panels of Fig 3).

The pattern of the change in trend of Dmn is different from that of Dmx, as shown in the bottom panels of Fig 3, where the values of the trend functions per decade mostly lie in the range (0.0, 0.3), and more stations have a cooling trend with negative values for trend functions. The trend function of the quantile 0.1 represents the change of temperature for the extremely cold days, 12 stations show a cooling pattern and six of these have been cooling $>0.1^{\circ}\text{C}$ per decade during the study period, i.e., station 12 and 13 in WA, 44 in QLD, 65 and 69 in VIC, and 72 in TAS. Nine stations show an increasing trend with $>0.3^{\circ}\text{C}$ per decade, i.e., station 3 in WA, station 26 in SA, six stations in QLD (station 31,34,36,39,41 and 42), and station 55 in NSW ($>0.4^{\circ}\text{C}$). For the quantile level 0.5, eight stations show a cooling trend in the south east and south west of Australia with negative values for the trend function, and four (stations 12, 44, 65 and 69) have been cooling $>0.1^{\circ}\text{C}$ per decade. Three stations (stations 3, 39 and 55) in WA and NSW show a warming trend of $>0.3^{\circ}\text{C}$. For the quantile level 0.9, only four stations still show a cooling trend with two (stations 12 and 13) in WA, one (60) in NSW

and one (63) in VIC. Three stations have an increasing trend $>0.3^{\circ}\text{C}$ degrees with one (station 3) in WA, two (stations 29 and 39) in QLD and one in NSW (station 67).

In terms of the trend function against quantile levels, Fig 4 and 4 display stations with any trend function $>0.3^{\circ}\text{C}$. Note that the red curve above the blue curve indicates that Dmx has increased more than Dmn, and vice versa. Trend values that increase with quantile level indicate larger variation in the series, and vice versa. A positive trend value in a high quantile of Dmx means more extreme heat events and a negative value of the trend function in a low quantile of Dmn means more extreme cold events.

For example, stations 4, 8, 20, 35, 38, 50, 52, 53, 59, 60, 61 and 72 in Fig 4 present such a pattern with the red curve above the blue curve. For station 4, larger quantiles increase more than smaller quantiles for both Dmx and Dmn with all >0 , indicating warming trend and bigger variation in both series, and more extreme heat events and less extreme cold events. Station 8 displays with warming trend but smaller variation in both series, while station 20 shows a warming trend in Dmx series with larger variation and more extreme heat events. In contrast, station 35 presents a warming trend with more extreme heat events but no larger variation in Dmx. Station 52 and 53 present a similar pattern with trend coefficient decreasing with quantile level in both series, which indicates a warming trend but smaller variation. Stations 60 and 61 have a warming trend in Dmx, but no clear trend in Dmn. Stations 50 and 59 have a warming trend in both series with smaller variation in Dmx.

Stations 3, 29, 31, 39 and 41 in Fig 4 have the blue curve above the red curve. Especially for station 31, the Dmx series present a cooling trend for trend coefficient of most quantile <0 and a smaller variation. The Dmn show a warming trend and a smaller variation. Although there are clear trends in both Dmx and Dmn, no such trend is appeared for the mean temperature, such trends might be difficult to obtain. For this station, extreme events occur less often.

Note that some stations have red and blue curves crossed. Examples are station 26, 35, 36, 42, 55 and 67, where at that quantile level both Dmx and Dmn have the same trend.

Spatial pattern of trend

The spatial pattern of trend functions across Australia is shown in Fig 5 for the trend of Dmx (in the top panels) and Dmn (in the bottom panels), respectively. For the 0.1 quantile of Dmx, the values of the trend function are all positive with a warming trend for cold days (after removing seasonality). The north-east area including NSW, VIC, TAS, the south part of QLD and east part of SA appear to experience more of an increase than other regions for the 0.1 quantile of Dmx, with $\geq 0.3^{\circ}\text{C}$ increase per decade in the last 60 years. This area covers most of the Murray–Darling basin, which experienced water loss in the last few years [27]. We especially highlight TAS and the greater Sydney area which have increased the most at nearly 0.4°C . In contrast, the far north QLD and the north-west corner of WA have experienced the least change with around 0.1°C increase in the same period. In terms of the 0.5 quantile of Dmx, TAS and parts of NSW still have mostly increasing temperatures with $>0.3^{\circ}\text{C}$, while other areas have 0.1°C to 0.3°C increase, except for the north of QLD and the north-west corner of WA showing a negligible increase of $\leq 0.1^{\circ}\text{C}$. When it comes to the 0.9 quantile, parts of the north of QLD also show a negligible increase, or even decrease. Other regions generally have a warming trend of 0.2°C to 0.3°C .

Trend in the Dmn series perform differently. For 0.1 quantile of Dmn, south QLD, a small region of north coast of WA, the coastal area near Sydney and Adelaide show a warming trend around $\geq 0.3^{\circ}\text{C}$. These areas continue to show a warming trend for the 0.5 quantile, but not for the 0.9 quantile. In contrast other regions have a smaller increase with $\leq 0.2^{\circ}\text{C}$ for the 0.1 quantile, and some areas (south-east and south-west region of Australia) even show a cooling

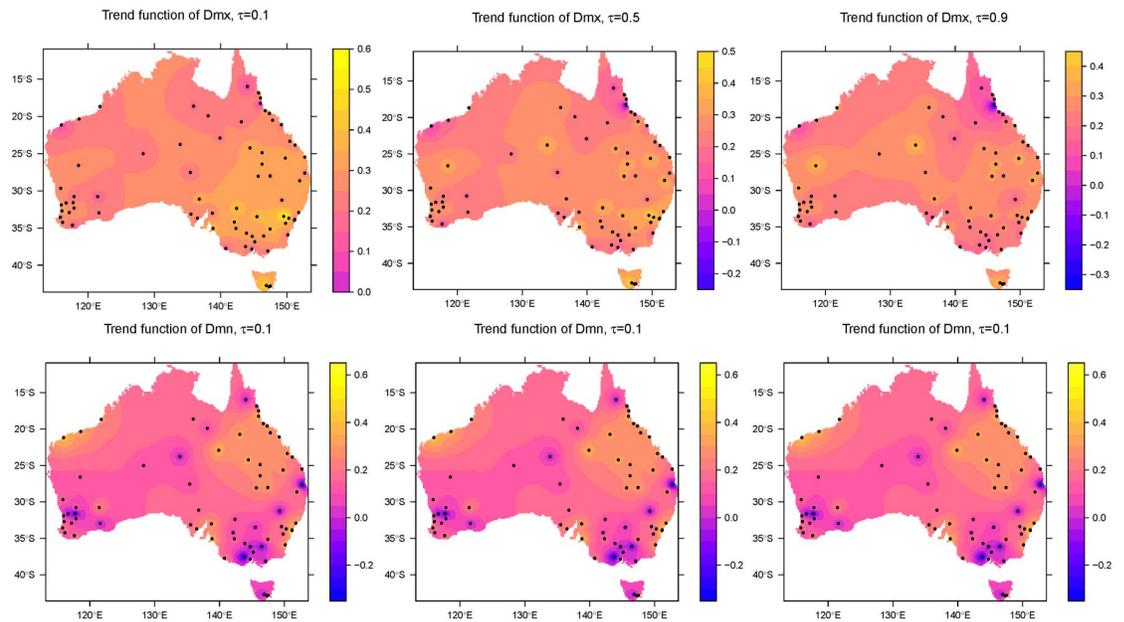


Fig 5. Quantile trend of $\tau = 0.1, 0.5$ and 0.9 for overall Australia during the study period. The color of point is the total degrees Celsius that increased/decreased per decade from 1960 to 2019. The top panels are for the Dmx series and the bottom panels are for the Dmn series.

<https://doi.org/10.1371/journal.pone.0271457.g005>

trend with a negative value of trend function. For 0.5 quantile, most parts of Australia do not show a large increase, with most values of trend function lying between 0 and 0.1°C , while the south-east area of the country experienced consistent cooling of time. However, no such cooling trend is shown for the 0.9 quantile. Instead, inland parts of QLD and north coast of WA show an increase with 0.3°C .

Discussion

This article has provided a detailed investigation of the changes in temperature across Australia in recent decades based on the original data set.

In this study, we raised the heterogeneity issue in the daily temperature time series with an exploratory analysis, where the intra-annual sample variance has quasi-periodic variations and temporal correlations. Such issues lead to inaccurate estimation of parameters coefficients, if they are not handled appropriately. Specifically, the trend detected might be misleading to a large extent. Many studies also suggest that the Long-range dependence (LRD) in a time series, if a time series displays a slowly declining autocorrelation function (ACF) in variance, can significantly increase the uncertainty of trend detection [14, 28–31]. Note that LRD can be also reflected in the ACF of residuals in a mean regression model. To include all the heterogeneity of variance into the model, GARCH model is used to model the variance of temperature time series. It has been shown that a GARCH model can also capture the shape of the ACF of volatility in daily financial return series, and is consistent with long-memory based on semiparametric and parametric estimates [32]. Hence, our variance model not only accounts for seasonality and temporal correlation, but also reduces the uncertainty caused by LRD.

In this study, spatio-temporal quantile regression has been applied to analyze the temperature series from 72 meteorological stations in Australia. By including the variance term as covariate in the quantile model, the proposed approach has considered a wide range of

heterogeneity including quasi-periodic variations and temporal correlations. We only include the linear trend in the modeling, since both linear and quadratic trend showed a similar pattern during the study period. However, this could be generated in other contexts.

Our results confirm the different patterns of climate change for different percentiles of daily maximum and minimum temperature series over Australia. Overall, the country appears to be experiencing a warming in daily maximum temperature except for a small area in far north QLD, and both cold and hot days are tending to become warmer. A warming trend in hot days will lead to more frequent extreme heat events. In general, NSW, south QLD and TAS experience the most significant warming in daily maximum temperature compared with other regions.

In terms of daily minimum temperature, South QLD and the north coast of WA experience more warming than other regions of Australia. However, the warming trend is less substantive than for daily maximum temperature. The daily minimum temperature series is associated with extreme cold events. Specifically, three areas, VIC, TAS and south WA have increasing numbers of extreme cold days. Notably, South QLD experiences an overall climate warming in both maximum and minimum temperature, leading to more frequent hot days and fewer cold days. The year round warming trends in South QLD may have significant adverse impacts on agricultural production in Queensland which is currently aiming to boost from AUD\$60 to 100 billion by 2030. The most populous state of Australia, NSW, is experiencing a climate warming in daily maximum temperature with more hot days, but stable daily minimum temperature. Our more southern states, VIC and TAS, have experienced more extreme weather, where VIC results much more extreme cold days and slightly more extreme hot days, while TAS has much more extreme hot days and slightly more extreme cold days. When we focus on summer, the eastern half of Australia, NSW, VIC, SA and south QLD, have experienced more warmer summer than other regions that have no substantive warming trend in summer. Winter generally gets warmer in most regions in Australia but gets less warmer in VIC with regard to daily maximum temperature. In daily minimum temperature series, QLD is becoming warmer, while other regions only are slightly warmer or even colder in south WA, NSW and VIC.

It is worth noting that our model results in different changing rates compared with these presented in regional reports [10, 33–38]. This is because these reports focused on the period between 1910 and 2013 and used a linear trend to obtain the changing rate. However, as noted in the report [39], most warming in Australia occurs after 1950 and the post-1950 period has a faster warming rate than the pre-1950 period.

It is also worth noting that the temperature data provided by `bomrang` is the original data. A homogenized or modified data set, called Australian Climate Observations Reference Network Surface Air Temperature (ACORN-SAT), has been provided by [40] and used to monitor the long-term temperature trend by the Bureau of Meteorology Australia. Our study uses the original temperature data set from R package `bomrang` rather than the homogenized version, because the trend coefficients of the extreme quantiles can be drastically affected by smoothing or modified outliers. This might lead to different results with some literature, especially on trend coefficients of the extreme quantiles at 0.1 and 0.9.

The interpretation of the spatial pattern of trend should consider the following limitations. The interpolation of spatial pattern was simply based on the distance to the selected stations, which are not distributed evenly as there are very few stations in the inland region of WA, NT and SA. Moreover, the impacts of geography, e.g., river catchment, mountain range and distance to ocean, are not accommodated in the analysis. This could lead to over-generalization of conclusions. However, these limitations do not affect the conclusions for selected stations.

Further visualization and analysis can be carried out using other statistics, for example local indicator of spatial association [41].

Finally, Our modeling has incorporated new components in climate data analysis and the proposed method can be applied to any other data sets. Our R code and source files are available at <https://github.com/ygwang2018/ClimateChange>.

Supporting information

S1 File. This supplementary document includes four sections, i.e., S1. Additional Figures for Exploratory Analysis, S2. Results of Inter-annual Variance Model, S3. Simulation Study and S4. Result of Quantile Trend by Season.

(PDF)

S2 File.

(ZIP)

Acknowledgments

The authors appreciated Professor Brian Reich for sharing the R code for the implementation of his spatio-temporal quantile regression model.

Author Contributions

Conceptualization: Glenn Brown, Kerrie Mengersen, You-Gan Wang.

Data curation: Qibin Duan.

Formal analysis: Qibin Duan.

Funding acquisition: Kerrie Mengersen, You-Gan Wang.

Investigation: Qibin Duan, Clare A. McGrory.

Methodology: Qibin Duan, Clare A. McGrory, You-Gan Wang.

Software: Qibin Duan.

Supervision: Kerrie Mengersen, You-Gan Wang.

Validation: Qibin Duan.

Visualization: Qibin Duan.

Writing – original draft: Qibin Duan, Clare A. McGrory.

Writing – review & editing: Glenn Brown, Kerrie Mengersen, You-Gan Wang.

References

1. Paik S, Min SK. Quantifying the anthropogenic greenhouse gas contribution to the observed spring snow cover decline using the CMIP6 multi-model ensemble. *Journal of Climate*. 2020;. <https://doi.org/10.1175/JCLI-D-20-0002.1>
2. Spinoni J, Barbosa P, Bucchignani E, Cassano J, Cavazos T, Christensen JH, et al. Future Global Meteorological Drought Hot Spots: A Study Based on CORDEX Data. *Journal of Climate*. 2020; 33(9):3635–3661. <https://doi.org/10.1175/JCLI-D-19-0084.1>
3. Stocker T, Dahe Q, Plattner GK. *Climate Change 2013: The Physical Science Basis*. Intergovernmental Panel on Climate Change (IPCC).; 2013.
4. Sinha B, Sévellec F, Robson J, Nurser AJG. Surging of Global Surface Temperature due to Decadal Legacy of Ocean Heat Uptake. *Journal of Climate*. 2020; 33(18):8025–8045. <https://doi.org/10.1175/JCLI-D-19-0874.1>

5. Alexander LV, Zhang X, Peterson TC, Caesar J, Gleason B, Klein Tank AMG, et al. Global observed changes in daily climate extremes of temperature and precipitation. *Journal of Geophysical Research: Atmospheres*. 2006; 111(D5). <https://doi.org/10.1029/2005JD006290>
6. Brown SJ, Caesar J, Ferro CAT. Global changes in extreme daily temperature since 1950. *Journal of Geophysical Research: Atmospheres*. 2008; 113(D5). <https://doi.org/10.1029/2006JD008091>
7. Zhang P, Ren G, Xu Y, Wang XL, Qin Y, Sun X, et al. Observed Changes in Extreme Temperature over the Global Land Based on a Newly Developed Station Daily Dataset. *Journal of Climate*. 2019; 32(24):8489–8509. <https://doi.org/10.1175/JCLI-D-18-0733.1>
8. CSIRO, Bureau of Meteorology Australia. State of the Climate 2020; 2020. Available from: <http://www.bom.gov.au/state-of-the-climate/>.
9. Bureau of Meteorology Australia. Annual climate statement 2019; 2019. Available from: <http://www.bom.gov.au/climate/current/annual/aus/>.
10. Ekström M, et al. Central Slopes Cluster Report, Climate Change in Australia Projections for Australia's Natural Resource Management Regions: Cluster Reports, eds. CSIRO and Bureau of Meteorology, Australia; 2015.
11. Koenker R, Bassett G. Regression Quantiles. *Econometrica*. 1978; 46(1):33–50. <https://doi.org/10.2307/1913643>
12. Koenker R, Schorfheide F. Quantile spline models for global temperature change. *Climatic Change*. 1994; 28(4):395–404. <https://doi.org/10.1007/BF01104081>
13. Barbosa SM, Scotto MG, Alonso AM. Summarising changes in air temperature over Central Europe by quantile regression and clustering. *Natural Hazards and Earth System Sciences*. 2011; 11(12):3227–3233. <https://doi.org/10.5194/nhess-11-3227-2011>
14. Gao M, Franzke CL. Quantile regression–based spatiotemporal analysis of extreme temperature change in China. *Journal of Climate*. 2017; 30(24):9897–9914. <https://doi.org/10.1175/JCLI-D-17-0356.1>
15. Franzke C. A novel method to test for significant trends in extreme values in serially dependent time series. *Geophysical Research Letters*. 2013; 40(7):1391–1395. <https://doi.org/10.1002/grl.50301>
16. Reich BJ. Spatiotemporal quantile regression for detecting distributional changes in environmental processes. *Journal of the Royal Statistical Society: Series C (Applied Statistics)*. 2012; 61(4):535–553. <https://doi.org/10.1111/j.1467-9876.2011.01025.x> PMID: 23861555
17. Bureau of Meteorology Australia. Climate Information (Australia); 2020. Available from: <http://www.bom.gov.au/climate/>.
18. Sparks AH, Padgham M, Parsonage H, Pembleton K. bomrang: Fetch Australian Government Bureau of Meteorology Weather Data. *The Journal of Open Source Software*. 2017; 2(17). <https://doi.org/10.21105/joss.00411>
19. Nicholls ZRJ, Meinshausen M, Lewis J, Gieseke R, Dommenges D, Dorheim K, et al. Reduced Complexity Model Intercomparison Project Phase 1: introduction and evaluation of global-mean temperature response. *Geoscientific Model Development*. 2020; 13(11):5175–5190. <https://doi.org/10.5194/gmd-13-5175-2020>
20. Gräler B, Pebesma E, Heuvelink G. Spatio-Temporal Interpolation using gstat. *The R Journal*. 2016; 8:204–218. <https://doi.org/10.32614/RJ-2016-014>
21. Campbell SD, Diebold FX. Weather forecasting for weather derivatives. *Journal of the American Statistical Association*. 2005; 100(469):6–16. <https://doi.org/10.1198/016214504000001051>
22. Benth FE, Benth JŠ. The volatility of temperature and pricing of weather derivatives. *Quantitative Finance*. 2007; 7(5):553–561. <https://doi.org/10.1080/14697680601155334>
23. Benth JŠ, Benth FE, Jalinskas P. A spatial-temporal model for temperature with seasonal variance. *Journal of Applied Statistics*. 2007; 34(7):823–841. <https://doi.org/10.1080/02664760701511398>
24. Sirangelo B, Caloiero T, Coscarelli R, Ferrari E. A stochastic model for the analysis of maximum daily temperature. *Theoretical and Applied Climatology*. 2017; 130(1-2):275–289. <https://doi.org/10.1007/s00704-016-1879-6>
25. Benth FE, Benth JŠ. Stochastic modelling of temperature variations with a view towards weather derivatives. *Applied Mathematical Finance*. 2005; 12(1):53–85. <https://doi.org/10.1080/1350486042000271638>
26. Chandler RE. On the use of generalized linear models for interpreting climate variability. *Environmetrics*. 2005; 16(7):699–715. <https://doi.org/10.1002/env.731>
27. Wentworth Group of Concerned Scientists. Assessment of river flows in the Murray-Darling Basin: Observed versus expected flows under the Basin Plan 2012-2019. Sydney, Australia; 2020.

28. Yue S, Pilon P, Phinney B, Cavadias G. The influence of autocorrelation on the ability to detect trend in hydrological series. *Hydrological processes*. 2002; 16(9):1807–1829. <https://doi.org/10.1002/hyp.1095>
29. Fatichi S, Barbosa SM, Caporali E, Silva ME. Deterministic versus stochastic trends: Detection and challenges. *Journal of Geophysical Research: Atmospheres*. 2009; 114(D18). <https://doi.org/10.1029/2009JD011960>
30. Franzke C. Long-Range Dependence and Climate Noise Characteristics of Antarctic Temperature Data. *Journal of Climate*. 2010; 23(22):6074–6081. <https://doi.org/10.1175/2010JCLI3654.1>
31. Franzke C. Nonlinear Trends, Long-Range Dependence, and Climate Noise Properties of Surface Temperature. *Journal of Climate*. 2012; 25(12):4172–4183. <https://doi.org/10.1175/JCLI-D-11-00293.1>
32. Maheu J. Can GARCH models capture long-range dependence? *Studies in Nonlinear Dynamics & Econometrics*. 2005; 9(4).
33. Moise A, et al. Monsoonal North Cluster Report, Climate Change in Australia Projections for Australia's Natural Resource Management Regions: Cluster Reports, eds. CSIRO and Bureau of Meteorology, Australia; 2015.
34. Timbal B, et al. Murray Basin Cluster Report, Climate Change in Australia Projections for Australia's Natural Resource Management Regions: Cluster Reports, eds. CSIRO and Bureau of Meteorology, Australia; 2015.
35. Watterson I, et al. Rangelands Cluster Report, Climate Change in Australia Projections for Australia's Natural Resource Management Regions: Cluster Reports, eds. CSIRO and Bureau of Meteorology, Australia; 2015.
36. Grose M, et al. Southern Slopes Cluster Report, Climate Change in Australia Projections for Australia's Natural Resource Management Regions: Cluster Reports, eds. CSIRO and Bureau of Meteorology, Australia; 2015.
37. Hope P, et al. Southern and South-Western Flatlands Cluster Report, Climate Change in Australia Projections for Australia's Natural Resource Management Regions: Cluster Reports, eds. CSIRO and Bureau of Meteorology, Australia; 2015.
38. McInnes K, et al. Wet Tropics Cluster Report, Climate Change in Australia Projections for Australia's Natural Resource Management Regions: Cluster Reports, eds. CSIRO and Bureau of Meteorology, Australia; 2015.
39. CSIRO, Bureau of Meteorology Australia. State of the Climate 2018; 2018. Available from: <http://www.bom.gov.au/state-of-the-climate/>.
40. Trewin B. A daily homogenized temperature data set for Australia. *International Journal of Climatology*. 2013; 33(6):1510–1529. <https://doi.org/10.1002/joc.3530>
41. Anselin L. Local Indicators of Spatial Association—LISA. *Geographical Analysis*. 1995; 27(2):93–115. <https://doi.org/10.1111/j.1538-4632.1995.tb00338.x>